Oxidation of Metals, Vol. 18, Nos. 1/2, 1982

The Influence of Superficially Applied Oxide Powders on the High-Temperature Oxidation Behavior of Cr_2O_3-Forming Alloys*

G. M. Ecer†, R. B. Singh,‡ and G. H. Meier§

Received May 28, 1982

The effects of superficially applied CeO_2, mixed rare earth oxides, Co_3O_4, and Cr_2O_3 powders on the isothermal and cyclic oxidation of Ni–Cr alloys and the effects of CeO_2 and MgO powders on the isothermal oxidation of Fe–25 wt.% Cr have been studied over the temperature range 940–1150°C in pure oxygen and dry air. The rates of oxidation of both the Ni- and Fe-base alloys were markedly reduced by the application of CeO_2 powder. The presence of CeO_2 also improved the scale adherence and resulted in marked changes in the oxidation morphology. The presence of Co_3O_4 or Cr_2O_3 powders on Ni–Cr alloys or MgO on Fe–Cr also produced changes in the oxidation morphology but did not decrease the rate of oxidation. These results are interpreted in terms of the influence of the oxide powders on the development of scale microstructure and their effectiveness in decreasing grain boundary transport in Cr_2O_3.

KEY WORDS: Nickel-chromium alloys; iron-chromium alloys; oxidation; cerium oxide; magnesium oxide.

INTRODUCTION

Small alloy additions of rare-earth elements and other oxygen-active elements have been found to alter the oxidation resistance of Cr_2O_3-forming alloys.[1–17] The effects of these additions usually include (i) formation of continuous Cr_2O_3 scales at lower alloy Cr concentrations, (ii) reduction in the rate of Cr_2O_3 growth, (iii) improved scale adhesion, (iv) change in the primary growth mechanism of the oxide from outward cation migration to

*This paper is based in part on the Ph.D. thesis of G. M. Ecer (1975) and in part on the M.S. thesis of R. B. Singh (1977).

†Smith Tool, Irvine, California 92713.
‡Colt Industries–Crucible Incorporated Midland, Pennsylvania 15059.
§University of Pittsburgh, Pittsburgh, Pennsylvania 15261.

0030-770X/82/0800-0055$03.00/0

inward anion migration, and (v) a reduction of the grain size in the Cr_2O_3 scale. Similar effects have also been observed when the oxygen-active elements are present as a fine oxide dispersion in the alloy prior to oxidation.[18–30]

Giggins and Pettit[18] explained these observations by suggesting that early in the oxidation, chromium is transported outward through the scale with the dispersoid accumulating at the metal–oxide interface and eventually blocking the transport and reducing the oxidation rate. Dissociation of Cr_2O_3 at this interface results in the inward movement of oxygen which results in the incorporation of the dispersoid into the scale. The outer Cr_2O_3 layer eventually disappears through CrO_3 volatilization. Stringer, Wilcox and Jaffee[21] postulated that dispersoid particles act as heterogeneous nucleation sites for oxide grains, reducing the internuclear distance, which allows more rapid formation of a continuous Cr_2O_3 film and produces a finer oxide grain size. The reduction in rate was explained as being due to the elimination of short-circuit diffusion paths for cations (probably dislocations) so that anion diffusion becomes rate-controlling. Grain-boundary diffusion is not considered to make a major contribution to scale growth.

Previous papers by two of the authors[13,31–33] on the oxidation of Ni-high Cr binary alloys and ternary alloys containing small additions of reactive elements showed that the major effects on scale growth are the extent of metal–oxide separation, void formation within the scale, and both lattice and short-circuit diffusion of reactants through the scale. Minor additions of reactive elements such as titanium and zirconium[33] and cerium[13] can affect Cr_2O_3 growth by altering the influence of any one of these variables. The influence of Ce additions, which were the most effective in decreasing the scale growth rate and improving scale adherence, were proposed[13] to be due to CeO_2 internal oxides serving as nucleation sites to produce a fine grained scale and Ce ions blocking grain boundary diffusion through the Cr_2O_3 scale.

The present paper describes additional observations of the oxidation of high-Cr Ni–Cr and Ni–Cr–Ce alloys and the effects of applying a dispersion of fine reactive-metal oxide particles to the surface of Ni–Cr and Fe–Cr alloys prior to oxidation.

EXPERIMENTAL

The primary alloys studied were nominally Ni–50 wt.% Cr and Fe–25 wt.% Cr (see Table I) although selected experiments were performed using other Ni–Cr alloys. The Ni–50Cr alloys were prepared by vacuum induction melting followed by hot-rolling, surface grinding, and cold-rolling

Table I. Chemical Analyses of Alloys Studied (wt.%)

Element	Ni–50Cr	Fe–25Cr
Nickel	bal.	0.13
Chromium	50.15	24.74
Iron	0.22	Bal.
Silicon	0.01	0.10
Copper	N.D.	0.005
Tungsten	N.D.	0.08

to a thickness of 0.9 cm. The alloy was homogenized in evacuated quartz capsules at 1200°C for 6 hr to stablize the grain size and then ground to a 600-grit surface to remove any Cr-depleted surface layers. The specimens were then stress-relieved for 5 min in evacuated capsules and water-quenched. The resulting slight discoloration of the surface was removed by lightly polishing on 600-grit paper. The Fe–25Cr alloys were vacuum arc melted and drop cast. The ingot was homogenized for 2 hr at 1000°C and then hot-rolled 67% to 0.3 cm thickness with two reheats at 1000°C. The alloy was reduced further to 0.06 cm by cold-rolling and annealed for 10 min at 875°C after which 0.003 cm was ground from each side to remove any Cr-depleted layer.

All alloy surfaces were ground to a 600-grit SiC finish and cleaned in alcohol prior to testing. Selected specimens were coated with dispersions of MgO, Cr_2O_3, Co_3O_4 and CeO_2 powders by dipping in an alcohol slurry of the oxide and air drying. The coating weights were generally on the order of 1 mg/cm^2. The alloys were oxidized at temperatures between 1000 and 1200°C either in air or oxygen with most of the exposures being carried out on a continuously weighing microbalance. Several thermal cycling experiments were also made.

Specimens were examined following exposure using conventional optical metallography, X-ray diffraction, and scanning electron microscopy.

RESULTS AND DISCUSSION

The rates of oxidation at 1000°C of bare Ni–50Cr and the same alloy coated with dispersions of Co_3O_4, Cr_2,O_3 and CeO_2 are indicated in Fig. 1. The dispersions of Co_3O_4 and Cr_2O_3 have rather little effect on the rate whereas CeO_2 is seen to markedly reduce the rate after extended time. The weight gain after 20 hr is 0.6 mg/cm^2 for the CeO_2-coated specimen as compared with 2.3 mg/cm^2 for the bare alloy. (In comparison, a Ni–49Cr–0.08Ce alloy showed a weight gain of about 0.25 mg/cm^2 under

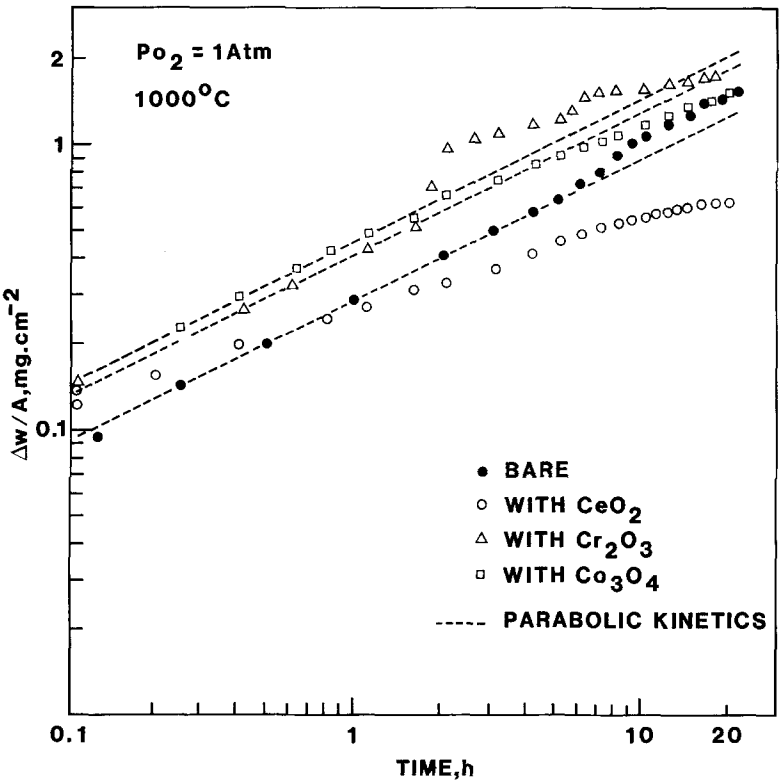

Fig. 1. Effect of CeO_2, Cr_2O_3, and Co_3O_4 particles applied to the surface of Ni–50Cr specimens on their oxidation rates at 1000°C in oxygen.

similar oxidation conditions.[13] The CeO_2-coated specimen is shown to deviate in a negative manner from a parabolic rate (dashed lines) as was also reported for Ni–Cr–Ce alloys.[13] Therefore, the external application of CeO_2 to Ni–50Cr appears to give qualitatively similar kinetic results to those for Ce added during melting of the alloy. The rate reduction does not appear to be due to the particles limiting the access of oxygen to the alloy since the Cr_2O_3- and Co_3O_4-treated specimens oxidized at rates comparable to or greater than that of the bare alloy.

The superficially applied oxide particles typically showed a nonuniform distribution both before and after oxidation as shown in Figs. 2 and 3. Many of the Cr_2O_3 particles have been incorporated into the growing scale (Fig. 3a) while the CeO_2 particles retained their identity and remained mostly attached to the outer scale surface (Fig. 3b). However, some of the

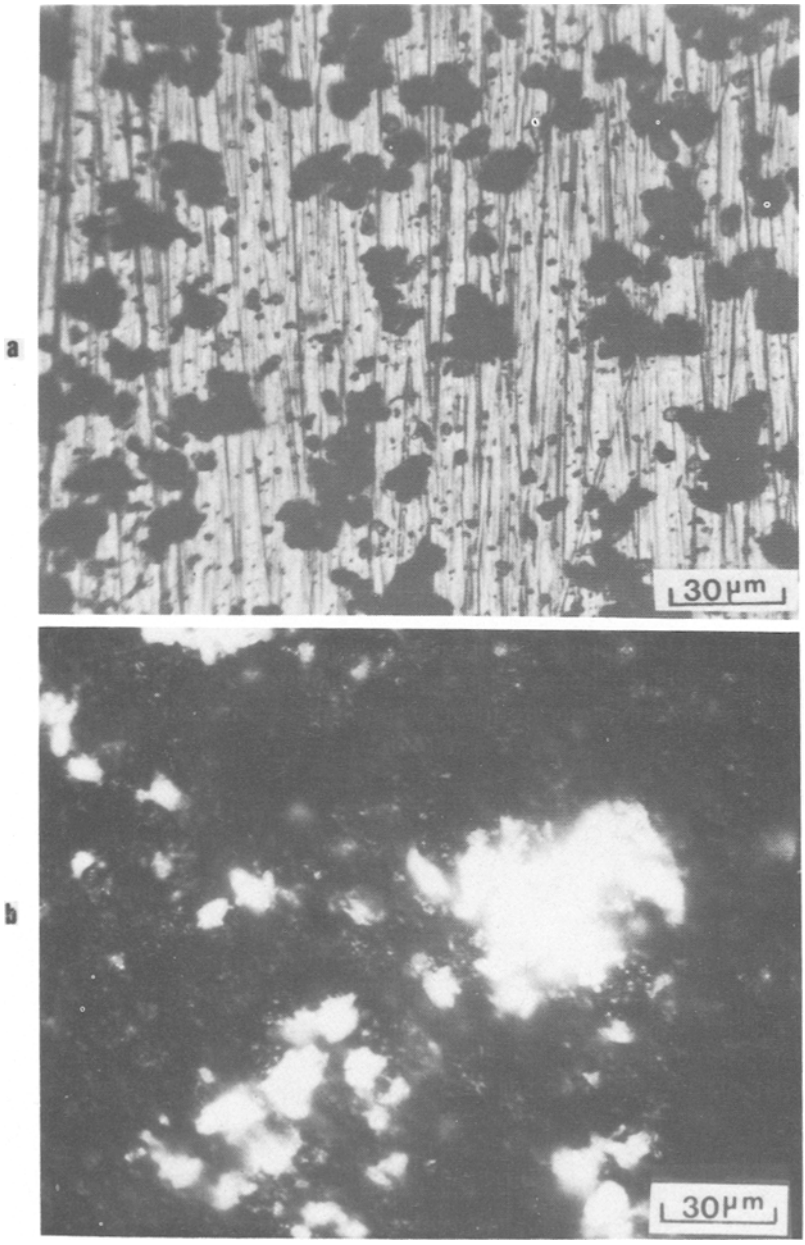

Fig. 2. Optical micrographs showing the distribution of CeO_2 particles applied to the surface of an oxidation test specimen prior to (a) and after (b) oxidation. The dark particles in (a) and the light particles in (b) are CeO_2.

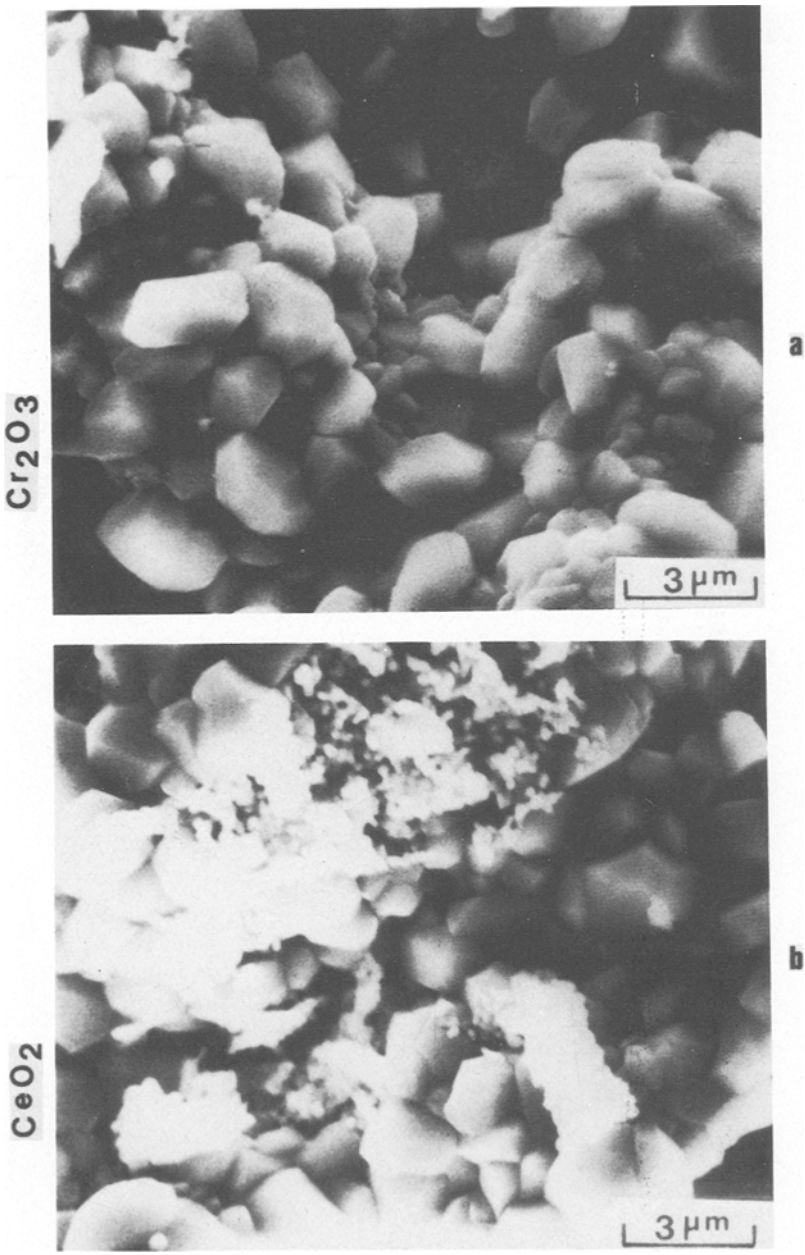

Fig. 3. Outer surface of the scale on a Cr_2O_3-applied Ni–50Cr specimen after 18 hr at 1000°C in oxygen (a) and outer surface of the scale on a CeO_2-applied Ni–50Cr specimen after 20 hr at 1000°C in oxygen (b).

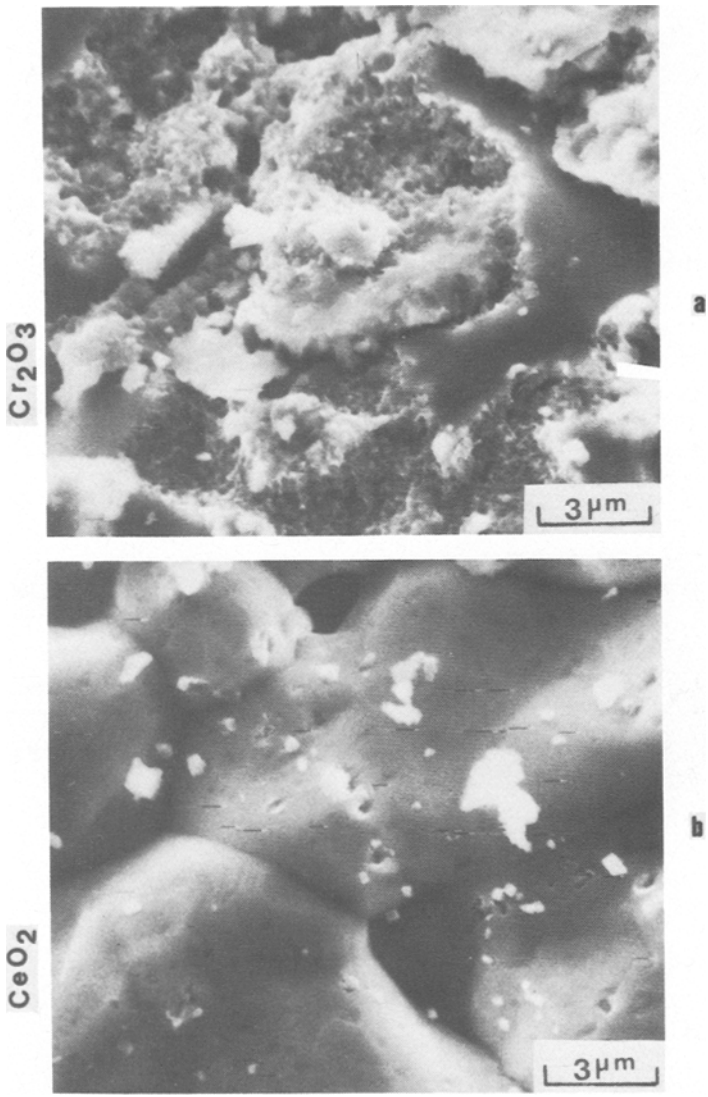

Fig. 4. Substrate surface of a Cr_2O_3-applied Ni–50Cr specimen after 18 hr at 1000°C in oxygen (a) and the substrate surface of a CeO_2-applied Ni–50Cr specimen after 20 hr at 1000°C in oxygen (b). The white particles in (b) are loosely attached CeO_2.

CeO_2 particles were found at the scale alloy interface (Fig. 4b) and some within the scale (Fig. 5).

The scale morphology was noticeably altered by the presence of the superficially applied oxides as seen in Figs. 5 and 6. The scale on the Co_3O_4 applied specimen had a fluffy outer layer at areas where the Co_3O_4 was present initially. This layer appeared to be $CoCr_2O_4$ formed by reaction between the particles and the Cr_2O_3 scale. A continuous Cr_2O_3 scale covered the alloy surface. Considerable porosity was observed at the scale–alloy interface and the porosity and some internal Cr_2O_3 was observed in the Cr-depleted region visible below the scale in Fig. 6a.

The Cr_2O_3-applied specimen showed a scale morphology typical of that reported for bare Ni–50Cr alloys.[32] This morphology consists of a slightly convoluted Cr_2O_3 scale which contains voids both within the scale and at the scale–alloy interface. The alloy is depleted of Cr below the scale as evidenced by the dissolution of the Cr-rich phase and voids are observed

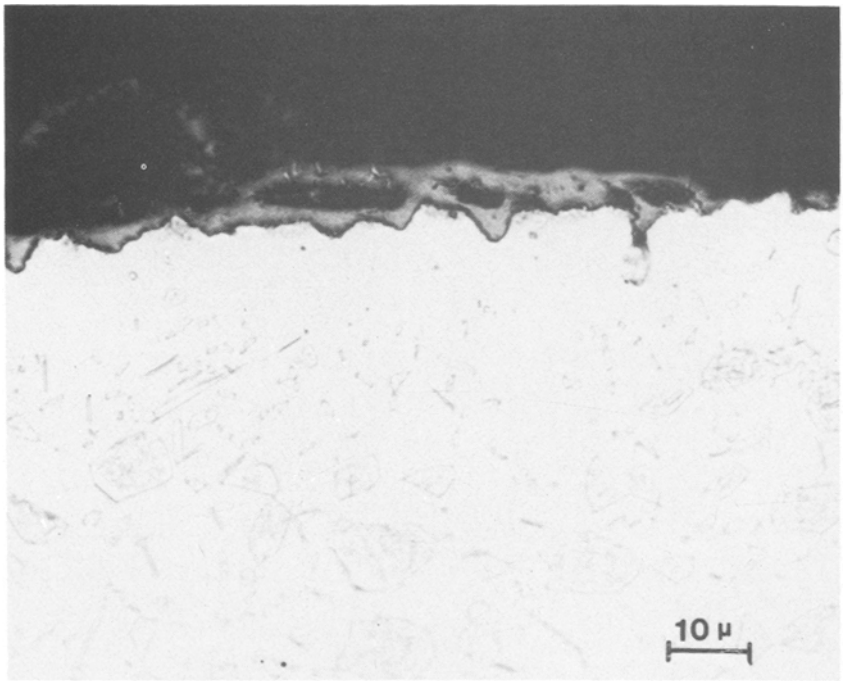

Fig. 5 Cross section of a CeO_2 applied Ni–50Cr specimen after 20 hr at 1000°C in oxygen. The white particles embedded in the scale are CeO_2 particles.

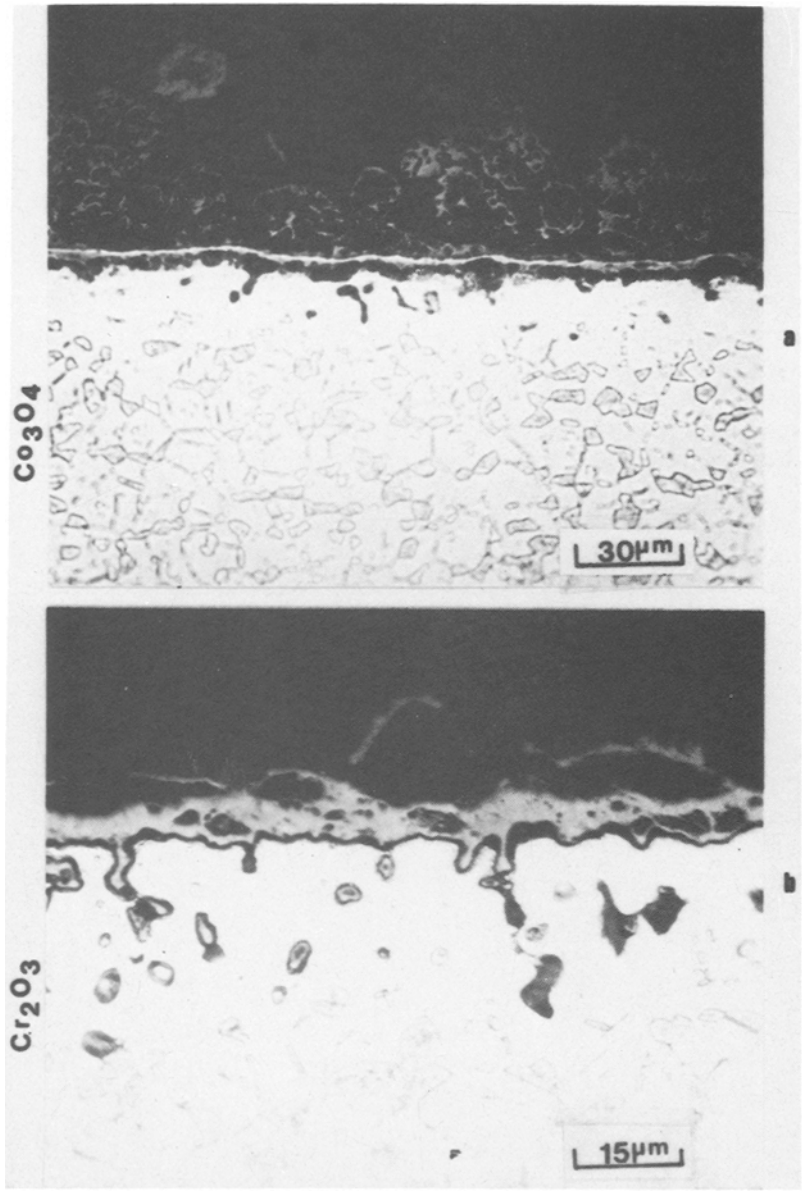

Fig. 6. Effect of superficially applied oxides on the scale morphology of Ni–50Cr specimens oxidized at 1000°C in oxygen. (a) Co_3O_4-applied specimen after 20 hr of oxidation. (b) Cr_2O_3-applied specimen after 18 hr of oxidation.

within this depletion zone. The voids on grain boundaries have been partially filled with Cr_2O_3 growing down from the continuous scale.

The CeO_2-applied specimen exhibited a thinner external scale and smaller Cr-depletion zone, both of which are consistent with the slower oxidation rate. Some voids were observed at the scale–alloy interface (Figs. 4b and 5) but few voids were detected in the alloy substrate and protrusion of the scale into the alloy was not extensive. The oxide grain size was about a factor of 2 smaller than that for the bare alloy. The oxidation morphology was qualitatively similar to that observed for Ni–50Cr–Ce alloys (see Fig. 7 and Ref. 13).

The scale morphology for the oxidation of bare Ni–50Cr, which is typical of that on the Cr_2O_3- and Co_3O_4-applied alloys, has been described previously.[32] Alloy–oxide separation takes place early in the oxidation process as the result of cation vacancy condensation. The separation allows the scale to bulge under the influence of compressive growth stresses and Cr-vapor transport across the voids is required for continued scale growth. Eventually, the bulged scale cracks, admitting oxygen to the alloy substrate where Cr_2O_3 again forms. The growth of this new scale and sintering to the old one results in the voids being incorporated into the scale. Recently, Shida *et al.*[34] analyzed the pores formed at the scale–alloy interface and

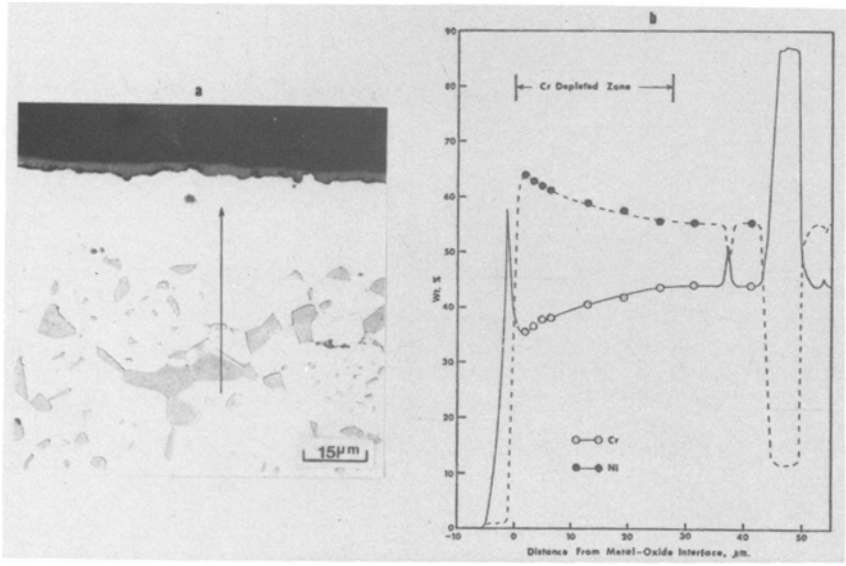

Fig. 7. (a) Ni–49Cr–0.08Ce alloy oxidized for 80 hr at 1100°C in oxygen. (b) Concentration profiles along the line of traverse indicated by the arrow in (a).

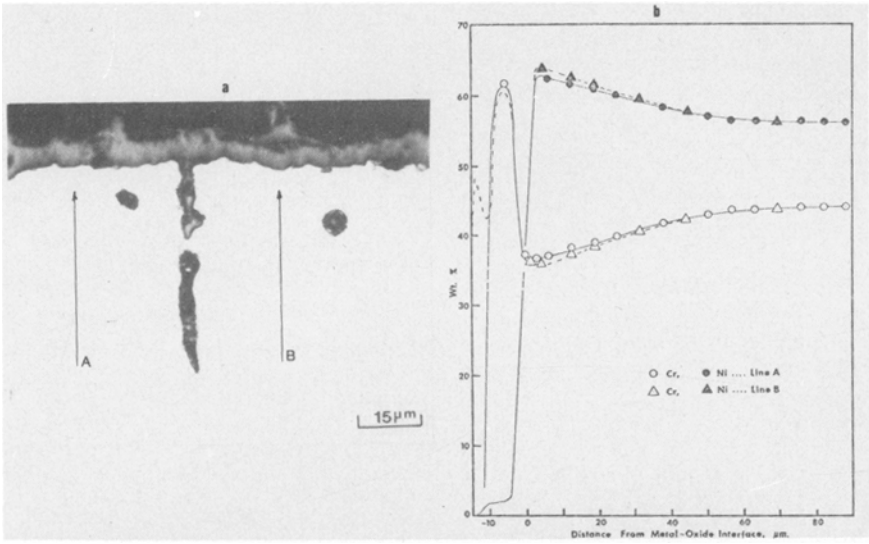

Fig. 8. (a) Ni–44Cr alloy oxidized for 22 hr at 1100°C in oxygen. (b) Concentration profiles along the lines of traverse indicated by the arrows in (a).

in the Cr-depleted zone for single-phase Ni–40Cr alloys which had been oxidized at temperatures between 1000 and 1200°C. At 1000 and 1100°C the pores were confined to the alloy grain boundaries and were partially filled with oxide. The pores were suggested to result from two processes: condensation of vacancies injected from scale growth and condensation of vacancies due to the Kirkendall effect in the interdiffusion of Ni and Cr in the Cr-depleted zone since $D_{Cr} > D_{Ni}$. The Cr_2O_3 in the pores was proposed to form by oxygen transported from the scale–metal interface, where the activity of Cr was low, down the pores to regions where the Cr activity was high enough to form Cr_2O_3. The deepest penetration of the Cr_2O_3 could be correlated approximately with the depth of the Cr-depleted zone. These observations are consistent with the results for the single-phase alloys studied here such as Ni–44Cr (Fig. 8). However, there are several differences for the two-phase Ni–50Cr alloys, both bare and coated with Co_3O_4 and Cr_2O_3. These are unoxidized pores in the grain centers (Figs. 6b and 9) and some small internal oxides in the grains in addition to the larger ones at grain boundaries. The latter feature can be seen more clearly in Fig. 10 which is a section taken parallel to and slightly below the scale–alloy interface of a Ni–50Cr alloy. The larger oxides are on alloy grain boundaries but the smaller ones have formed within the grains. The mechanism proposed by Shida *et al.* appears to be operative but the higher

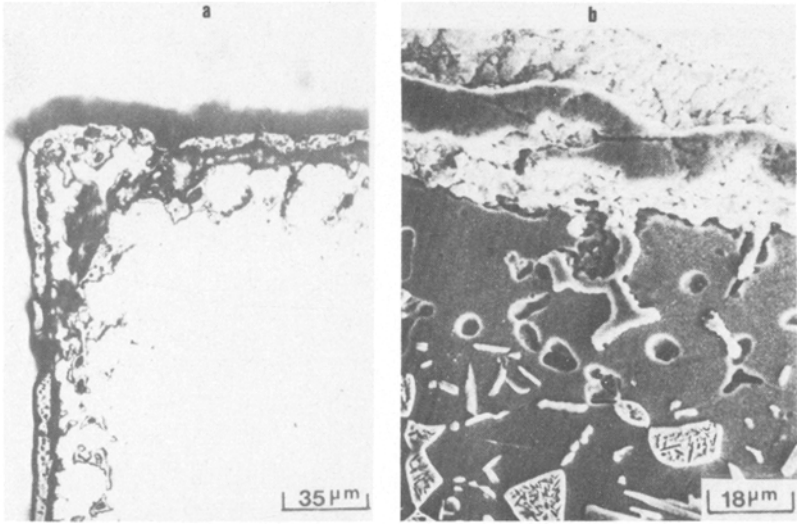

Fig. 9. Cross sections through a Ni–50Cr specimen oxidized for 20 hr at 1100°C and quenched in bismuth to maintain scale in contact with the substrate.

alloy Cr concentration results in internal Cr-oxide formation by the inward diffusion of oxygen through the alloy grains as well as along grain boundaries. Also, the vacancies, produced by injection and the Kirkendall effect, condense out in the alloy grains as well as in the grain boundaries. The presence of Ce in the alloy (Fig. 7) or CeO_2 application to the surface (Fig. 5) suppresses the formation of voids in the substrate and internal oxides even though Cr depletion has occurred. This result is due primarily to the slower oxidation rate resulting in fewer cation vacancies arriving at the scale–alloy interface and less Cr depletion. The Ce contained in the alloy was observed to oxidize internally but it is not believed that these particles have acted as vacancy sinks since the surface application of CeO_2 produced the same result.

The influence of externally applied CeO_2 on the kinetics and morphology of oxidation for Ni–50Cr alloys can be explained by the same mechanism proposed previously for the effects of Ce contained in the alloy,[13] i.e., the incorporation of CeO_2 into the scale reduces oxide grain growth and the adsorption of Ce ions to oxide grain boundaries blocks short-circuit diffusion. The transport blocked is apparently that of anions since considerable separation still occurs at the scale–alloy interface. The reduction of anion mobility reduces the compressive stresses in the scale resulting in less buckling. This effect is consistent with the recent observation

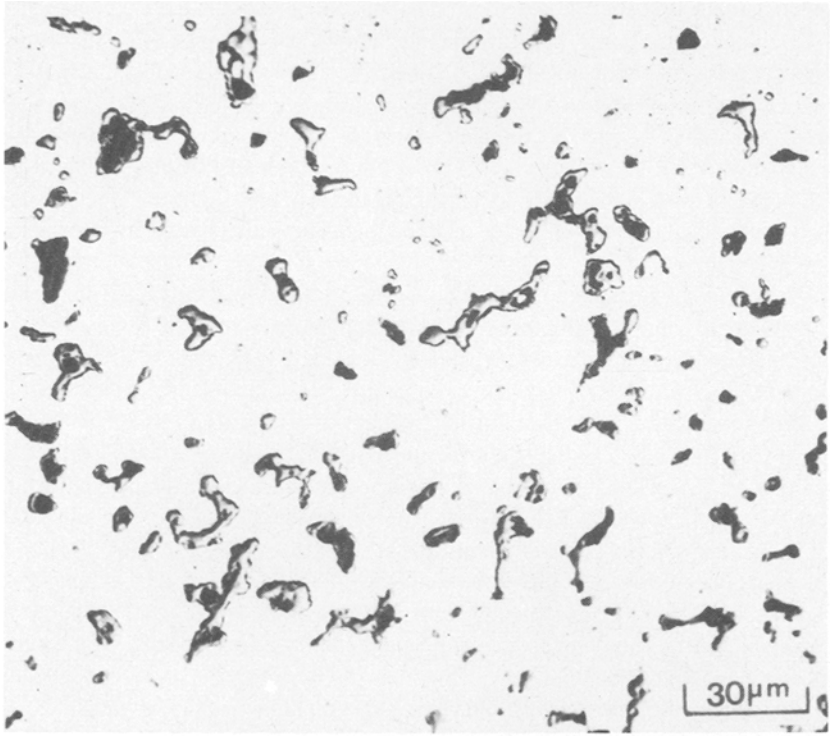

Fig. 10. Ni–50Cr oxidized for 22 hr at 1100°C in air. Micrograph corresponds to a plane parallel to and 10–15 μ below the alloy–oxide interface. The large oxide particles and voids are located at grain boundaries while smaller ones are within the grains.

of Delaunay *et al.*[35] who found that compressive growth stresses calculated from the bending of Ni–34Cr specimens oxidized on only one side were reduced for a given oxide thickness by the addition of yttrium to the alloy. This was explained by Delaunay *et al.* in terms of enhanced scale plasticity. Indeed the finer oxide grain size observed on both Y- and Ce-modified alloys may deform more readily at high temperatures but the reduction in anion diffusion explains both the reduced stresses and reduced growth rate. The fact that Ce and Y are effective in blocking grain-boundary transport while Cr and Co are not is believed to be due to a stronger grain-boundary adsorption of the former ions because of their large size mismatch in the Cr_2O_3 lattice.

An alternative explanation of the effect of Ce and CeO_2 in reducing the rate of Cr_2O_3 growth would be that Ce exerts a doping effect on Cr_2O_3.

Kofstad and Lillerud[36] have interpreted oxidation data for pure Cr in terms of Cr interstitials being the predominant ionic defect in Cr_2O_3 at oxygen partial pressures near the Cr/Cr_2O_3 equilibrium. If this defect model is correct, Ce^{+4} ions dissolving into Cr_2O_3 could result in a decrease in the concentration of Cr interstitials and a corresponding decrease in the transport rate of Cr ions through a Cr_2O_3 scale. However, the observation that Y, which should not result in a doping effect, has similar effects to Ce suggests that a doping effect is not the predominant factor in decreasing the Cr_2O_3 growth rate.

Limited thermal cycling experiments indicated that surface application of rare-earth oxides reduced scale spalling from Ni–50Cr. The effect of coating with mischmetal oxide (mainly Ce and La oxides) is illustrated in Table II. The reduction in spalling is certainly due partially to lower thermal stresses associated with the thinner scale on the rare-earth oxide-coated alloy. However, the stress measurements by Delaunay *et al.*[35] indicated that the growth stresses for Ni–34Cr were added to the compressive thermal stresses on cooling. Therefore, the lower growth stresses associated with the blocking of anion diffusion and the ability of the finer grained scale to, presumably, relieve growth stresses better may well be a second factor associated with rare-earth-containing alloys and the rare-earth oxide-coated alloys having better resistance to spalling. Long term experiments have not been conducted to determine the length of time superficially-applied oxides will remain effective.

Fe–Cr Alloys

Most of the experiments with Fe–25Cr alloys were done with superficial application of MgO particles. Figure 11 shows the rate of air oxidation of bare and MgO-coated Fe–25Cr at three temperatures. The presence of the MgO is seen to have a negligible effect on the kinetics at 1150°C and

Table II. Cyclic Oxidation of Ni–50Cr with and without Mischmetal Oxide Application at 940°C in 1 atm of Air.

		Specimen without MMO		Specimen with MMO	
Cycle	Time (hr)	Δw/A (mg/cm^2)	Observed spalling	Δw/A (mg/cm^2)	Observed spalling
1	17	+0.312	40%	+0.084	None
2	3	+0.130	negligible	0	None
3	19	+0.134	30%	+0.042	None
Total		+0.567	—	+0.126	

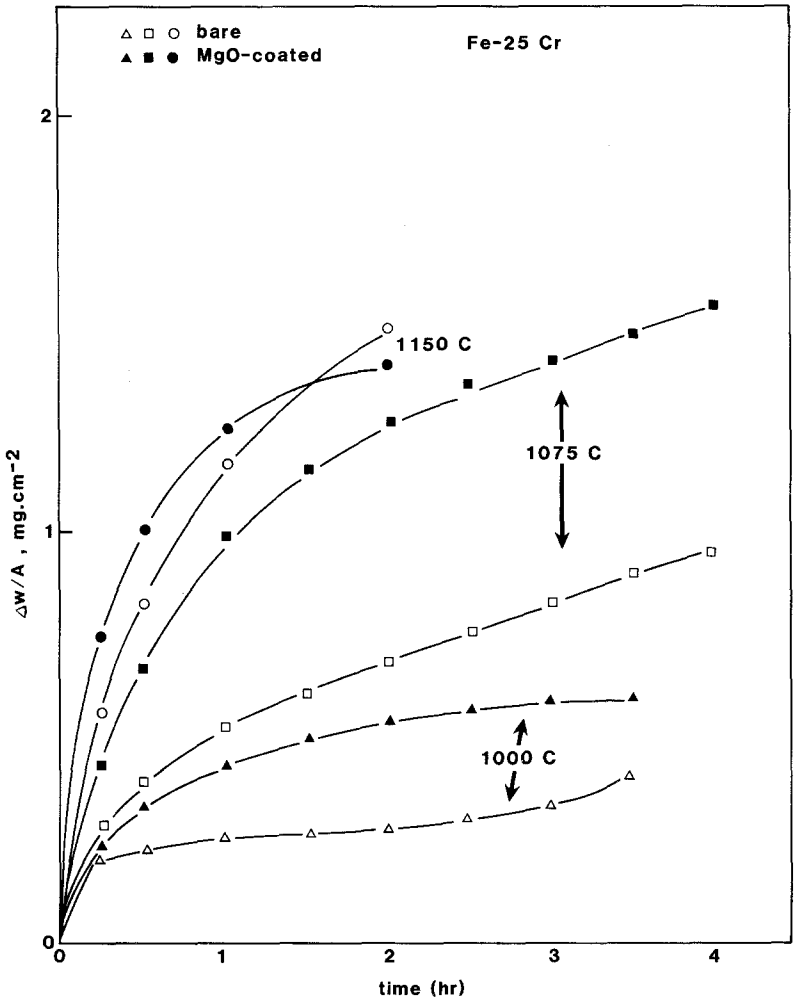

Fig. 11. Effect of superficially applied MgO powder on the oxidation rate of Fe–25Cr in air.

to slightly accelerate them at 1075 and 1000°C. The results for longer time experiments (to 144 hr) were qualitatively the same. The cause of the slight acceleration is not certain but may be due to changes in the Cr_2O_3 scale morphology (to be described) or to slightly enhanced CrO_3 evaporation with the MgO particles acting as a sink for CrO_3 to form $MgCr_2O_4$. (Such an effect has been identified when Cr_2O_3-forming alloys are heated in crucibles containing MgO.[37])

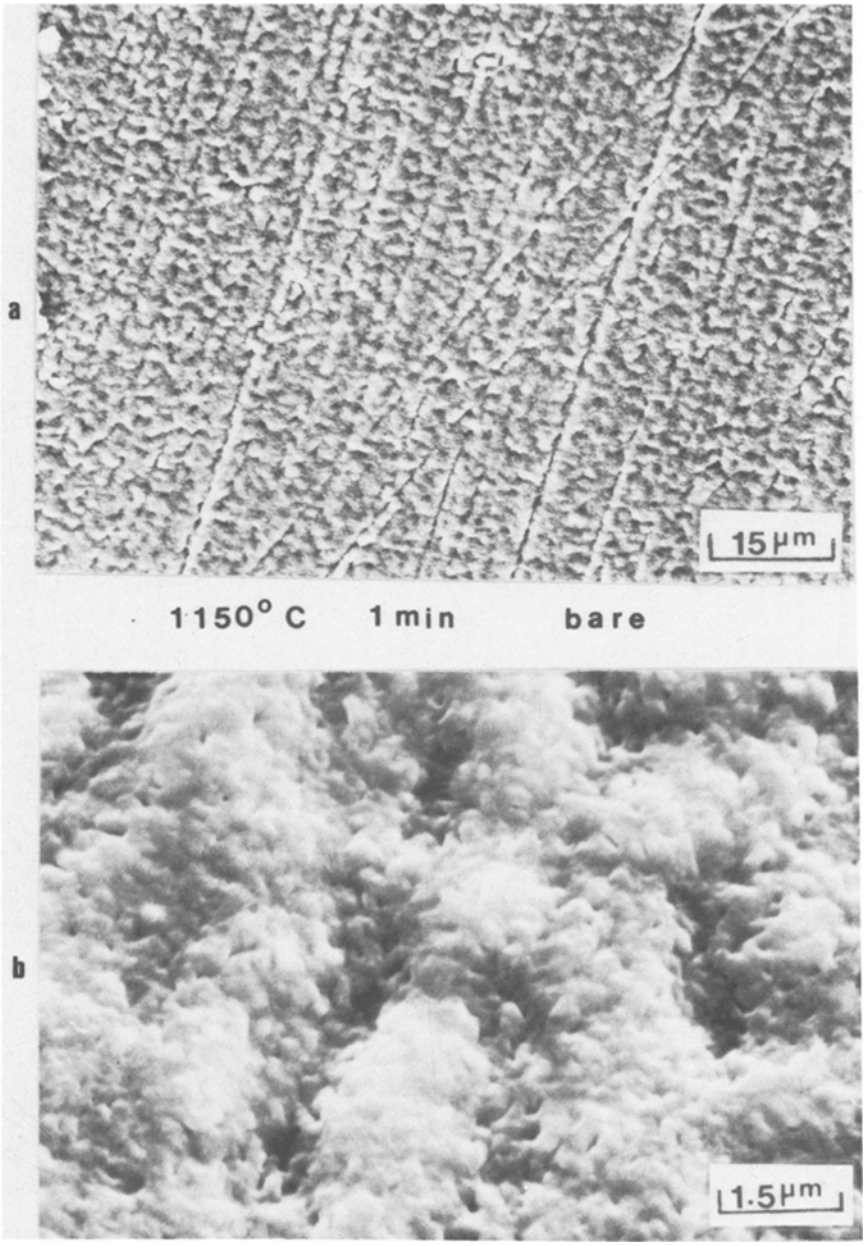

Fig. 12. Scale–gas interface of Fe–25Cr (without MgO) oxidized for 1 min in air at 1150°C.

The MgO produced significant differences in the oxide morphology as illustrated in Figs. 12–16. After one minute the oxide on the bare alloy (Figure 12) clearly replicated the polishing marks on the alloy and was shown by energy dispersive X-ray analysis to contain a significant amount of Fe as well as Cr. The oxide on the MgO-coated alloy (Fig. 13a) was finer grained, contained virtually no Fe, and gave little evidence of the underlying polishing lines. The presence of Mg-containing oxide was observed at the scale–gas interface. Figure 13b shows an area of the specimen where MgO was not detected. Here the scale morphology is similar to that in Fig. 12.

Figure 14a shows the surface of a bare alloy oxidized for 5 min where the scale has partially spalled. The alloy substrate is smooth indicating the scale had lost contact at temperature. Figure 15a shows a similar area on a MgO-coated specimen. Here the substrate is seen to contain a large number of points at which contact had been maintained with the scale at temperature. This difference in morphology is consistent with the observation that only a few spalled areas were present on the MgO-coated specimen while more than half of the uncoated specimen showed spalling. Figures 14b and 15b show the scale–gas interface for the two specimens at high magnification. The scale on the bare alloy contains significant amounts of Fe and is rather porous and wavy. The scale on the MgO-coated alloy is smooth and fine grained and contains only a trace of Fe. The scales on both alloys contain two layers indicated by the arrows in Figs. 14a and 15a.

Figure 16 shows the oxidation morphology for a MgO-coated (16a) and bare (16b) specimen exposed for 5 hr at 1075°C. The MgO-coated specimen exhibits a relatively flat scale–gas interface and a honeycomb-like substrate surface indicating a large number of contact points with the scale. Some grooving of the alloy grain boundaries from vacancy condensation is also evident. The layered nature of the scale is also apparent in Fig. 16a. The outer layer (arrows at A) was found to be essentially Cr_2O_3 but containing small amounts of Fe and Mg while the inner layer (arrows at B) was Cr_2O_3 with no evidence of Fe or Mg. The scale on the bare specimen (Figure 16b) showed a more buckled appearance and the substrate indicated there had been less scale–alloy contact at the oxidation temperature.

Therefore, the application of MgO prior to oxidation does not significantly alter the oxidation kinetics of Fe–25Cr but it has significant effects on the oxidation morphology. The major effect is the nucleation of a fine-grained Cr_2O_3 scale which maintains better contact with the alloy that minimizes buckling of the scale and reduces the extent of spalling on cooling.

In light of the effectiveness of CeO_2 application in reducing the oxidation rate of Ni–50Cr a number of Fe–25Cr specimens were oxidized in air

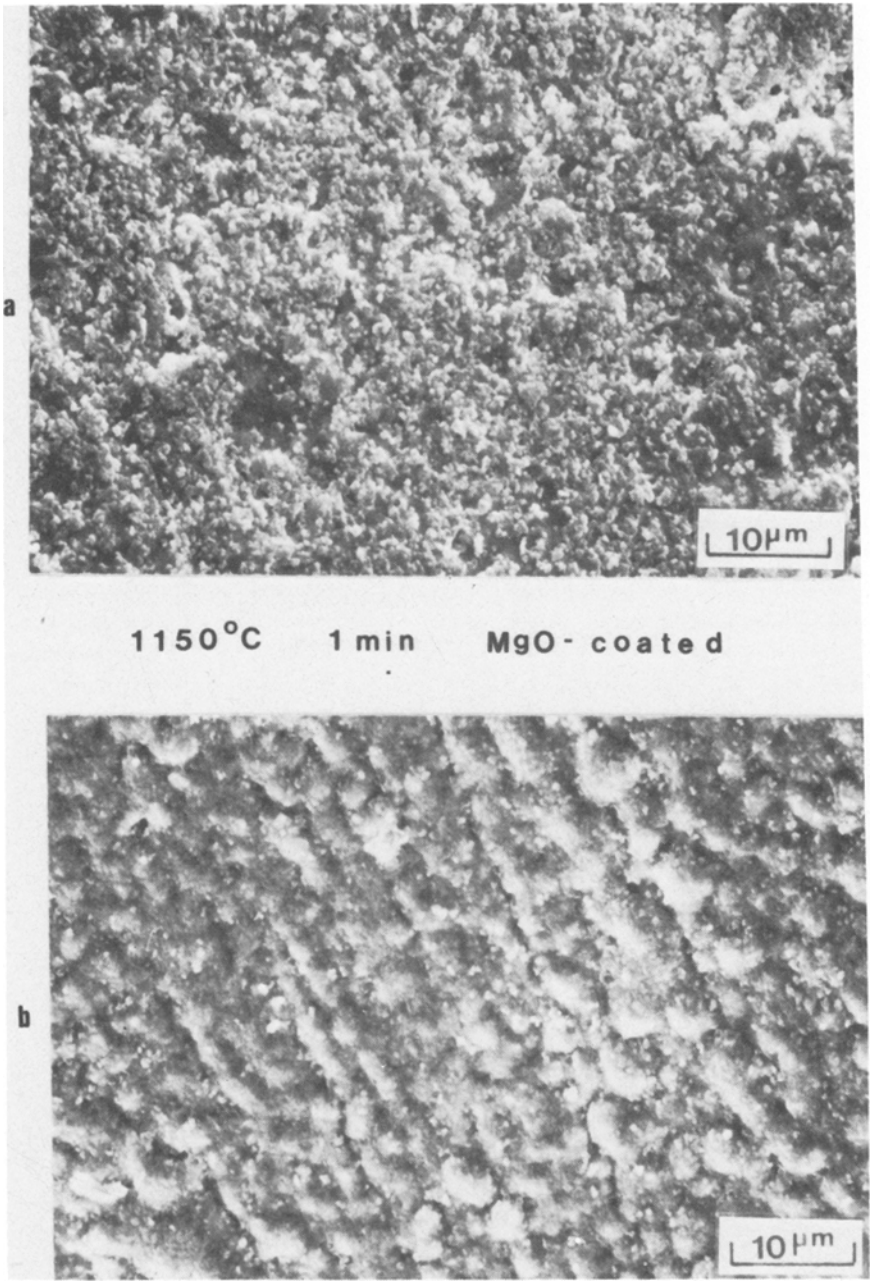

Fig. 13. Scale–gas interface of MgO-applied Fe–25Cr oxidized for 1 min in air at 1150°C.

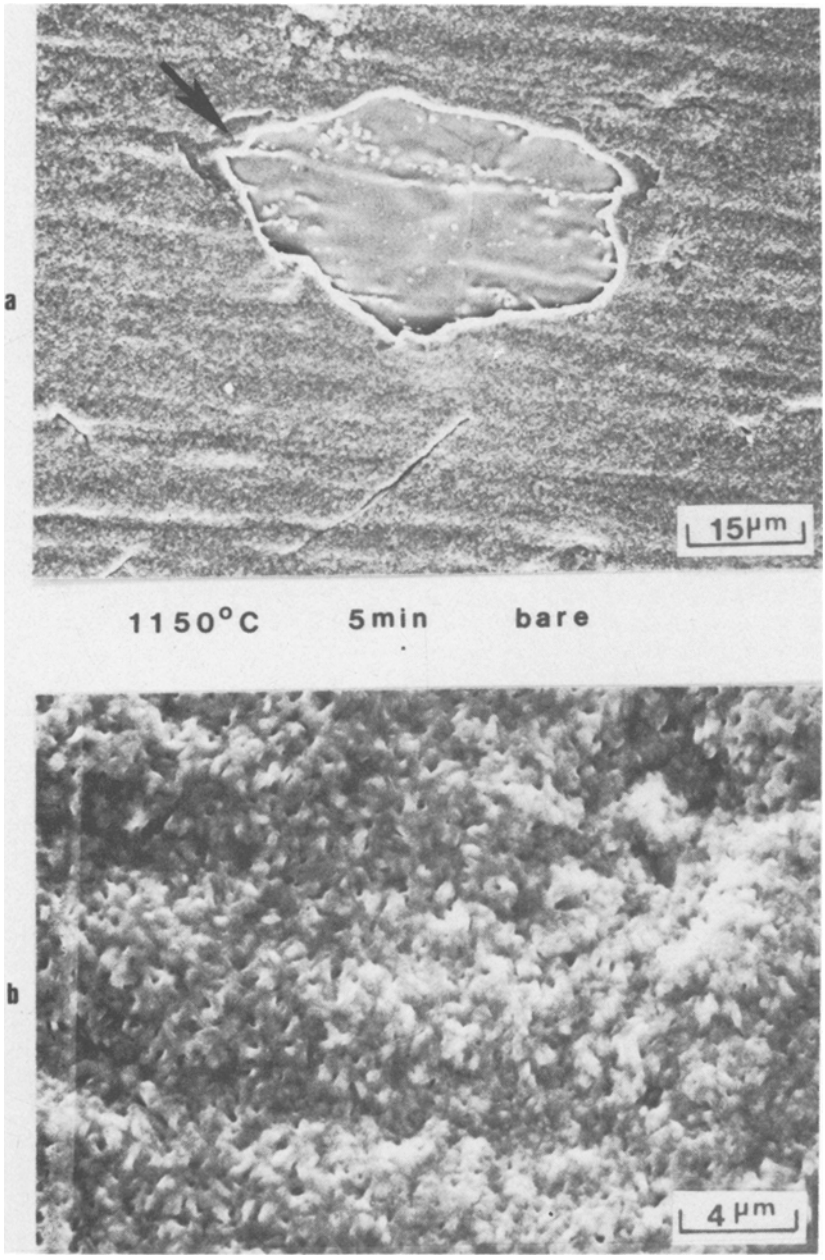

Fig. 14. Scale–gas interface of Fe–25Cr (without MgO) oxidized for 5 min in air at 1150°C.

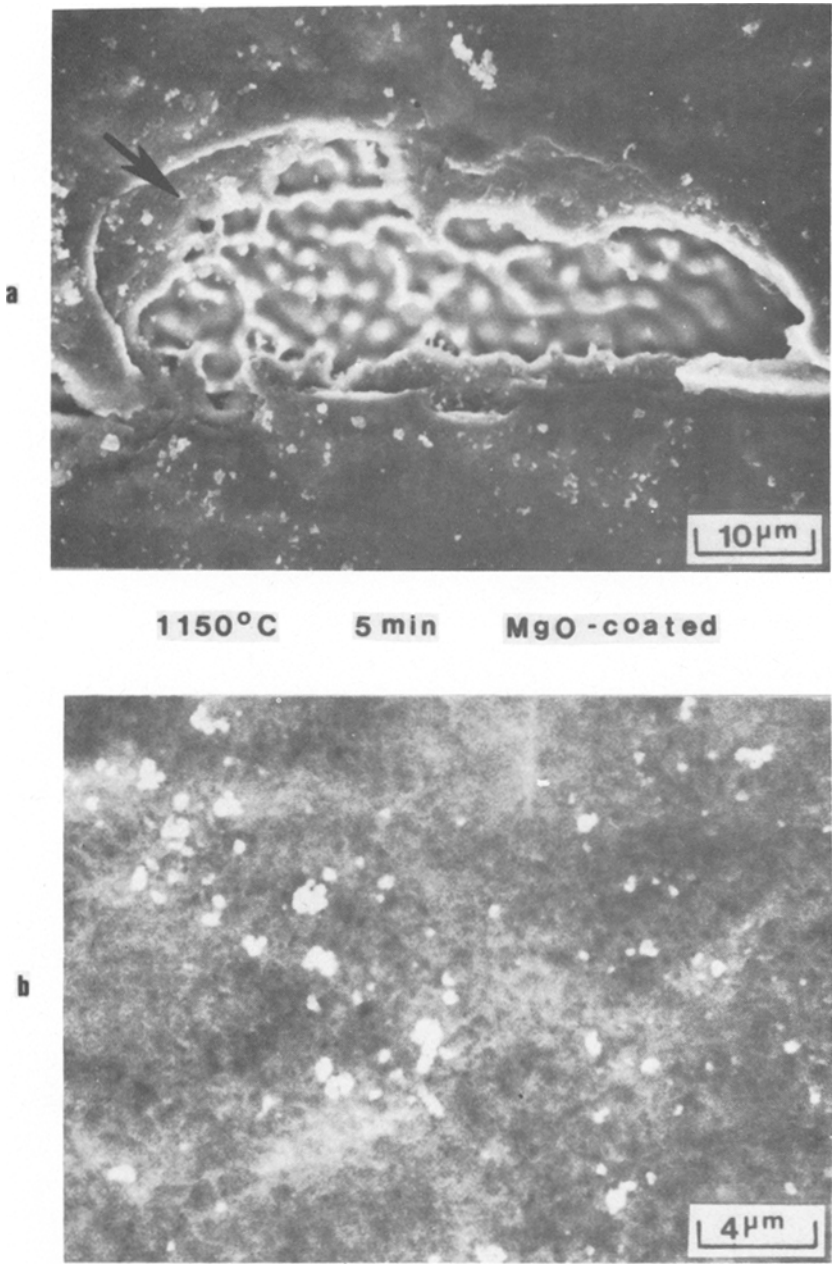

Fig. 15. Scale–gas interface of MgO-applied Fe–25Cr oxidized for 5 min in air at 1150°C.

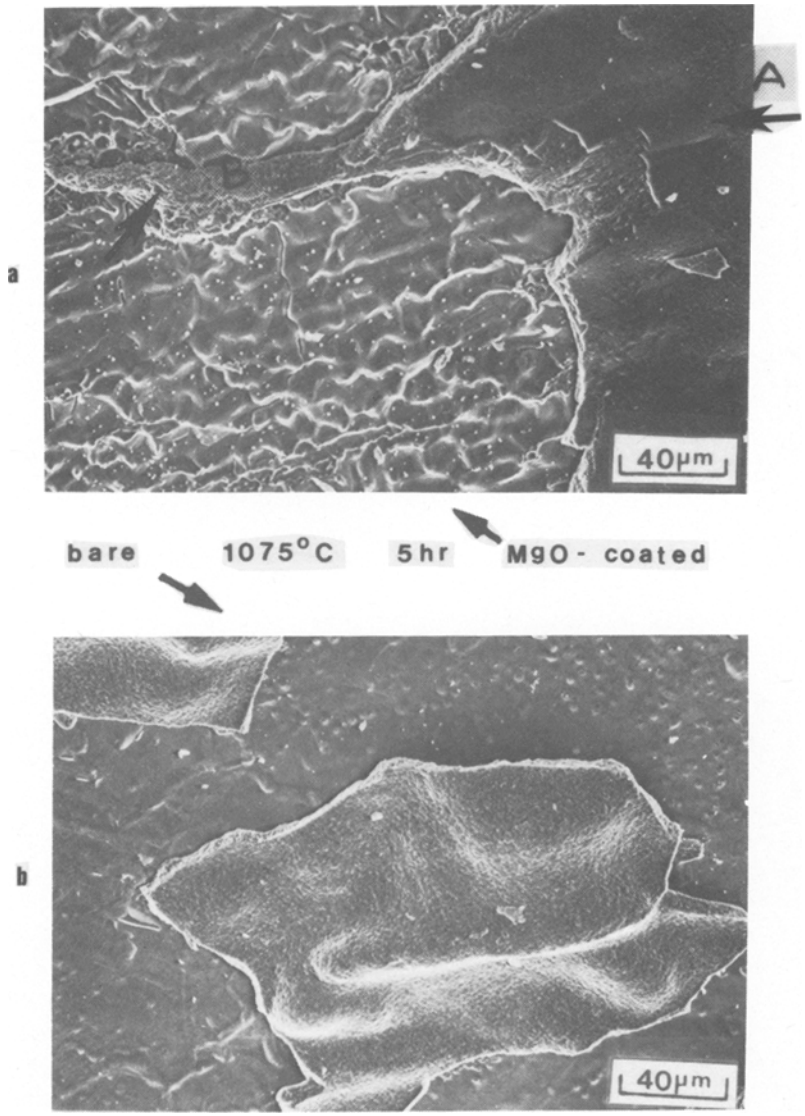

Fig. 16. Surface of Fe–25Cr alloys oxidized 5 hr in air at 1075°C: (a) with MgO application, (b) without MgO application.

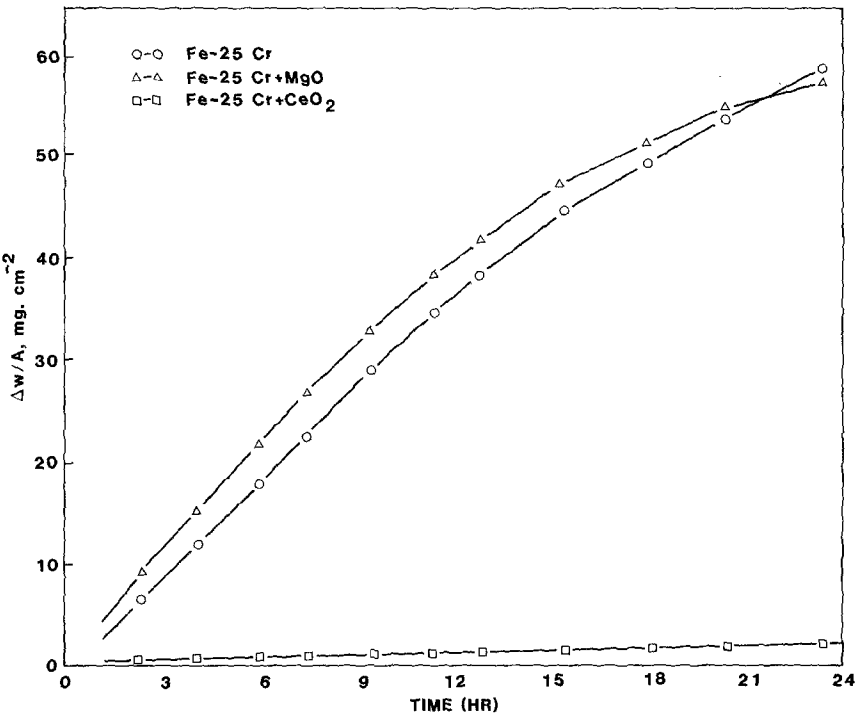

Fig. 17. Oxidation rates for three Fe–25Cr alloys in air at 1150°C.

at 1150°C with 1 mg/cm^2 coatings of CeO_2. Figure 17 shows a comparison between the oxidation for these specimens and those exposed bare and with MgO coatings. The CeO_2 application resulted in a remarkable decrease in the rate of oxidation which was quite reproducible on duplicate runs. The scale formed on the CeO_2-applied alloy was fine-grained Cr_2O_3. The surface of the specimen in Fig. 19a which was exposed for 1 min shows little influence of the polishing lines on the underlying alloy. Energy dispersive X-ray analysis of this surface revealed a considerable signal for iron but this is believed due to X-rays generated in the substrate as the signal decreased greatly for a 5 min oxidation and at longer times was not observed. The scale on a specimen exposed for 25 hr is seen in Fig. 18b. The grain size of Cr_2O_3 was less than 1 μ which is at least a factor of 5 smaller than that for a scale formed on a bare alloy for the same time (Fig. 19). The scale remained completely adherent on the CeO_2-applied alloy. Another important difference between the CeO_2-applied alloy and the bare alloy was the appearance of spikes of Fe oxides at the scale gas

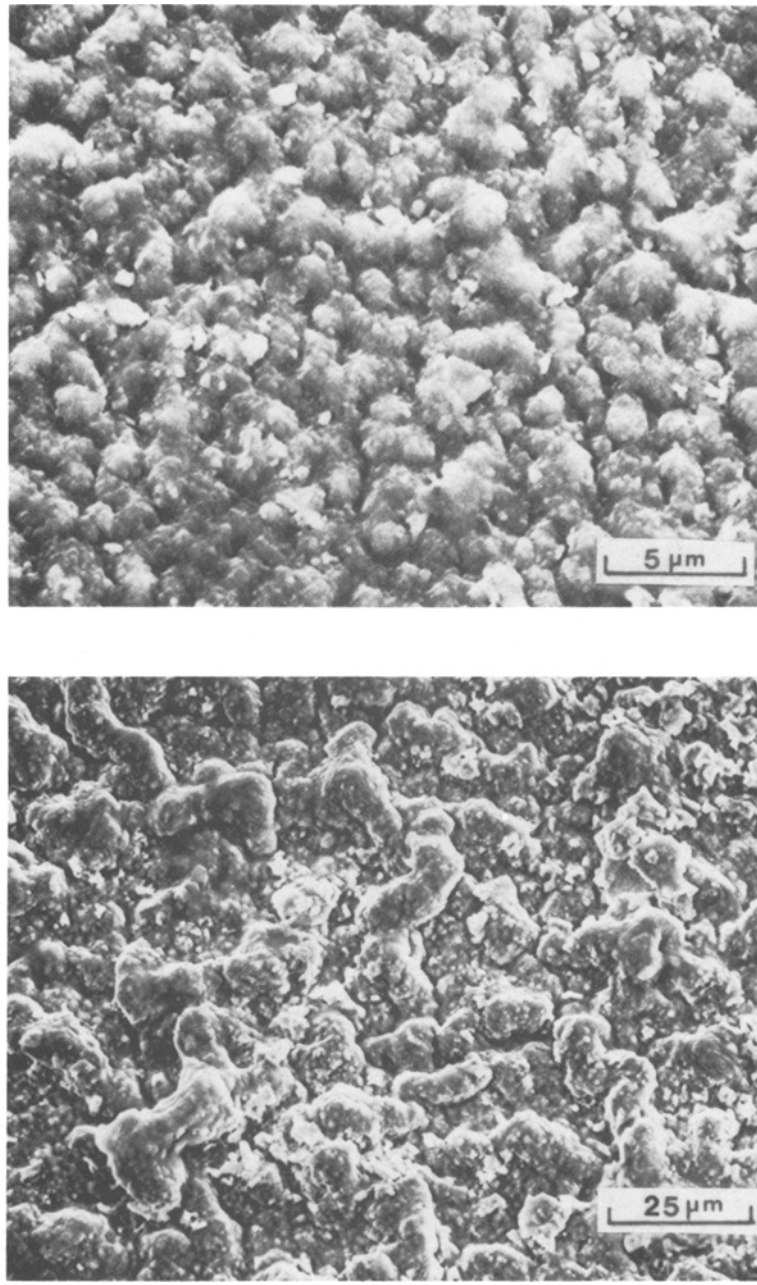

Fig. 18. Scale–gas interface for CeO_2-applied Fe–25Cr alloys oxidized in air at 1150°C. (a) 1 min and (b) for 25 hr.

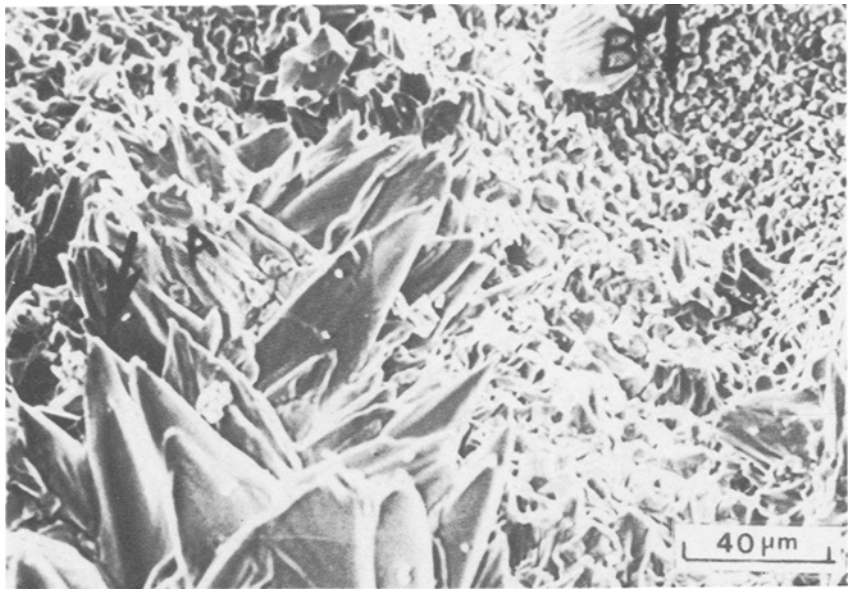

Fig. 19. Scale–gas interface for an Fe–25Cr alloy oxidized for 25 hr at 1150°C in air.

interface for the bare alloy after extended oxidation times (area A in Fig. 19). These features are the result of Cr depletion of the alloy below the alloy–scale interface and the corresponding increase in the activity of iron which results in significant transport of iron outward through the scale. These Fe oxide spikes were totally absent from the CeO_2 applied specimens due primarily to the slower oxidation rate causing less Cr depletion.

The slow rate of oxidation of the CeO_2-coated alloys was maintained to times in excess of 100 hr. However, one specimen was oxidized for 137 hr. For this specimen the rate started to increase after 100 hr and extensive scale spalling occurred on cooling. The weight gain after 137 hr for this specimen was still about a factor of 10 less than that for a comparable bare Fe–25Cr alloy.

Therefore, the presence of a fine dispersion of CeO_2 on the surface of Fe–25Cr results in the rapid formation of a fine-grained Cr_2O_3, greatly reducing the formation of transient Fe oxides, and reduces the growth rate of the Cr_2O_3. As in the case of Ni–50Cr the reduction in growth rate appears due to Ce blocking grain-boundary diffusion of anions through the scale. The ineffectiveness of MgO in decreasing the growth rate is likely due to a smaller tendency for Mg ions to segregate to Cr_2O_3 grain boundaries since the Mg ions ($r_{Mg^{2+}} = 0.65$ Å) fits rather well, from a size

standpoint, on Cr sites in the lattice ($r_{Cr^{3+}} = 0.6$Å). The size factor has been indicated to be the major factor in determining the extent of grain boundary adsorption of impurities in oxides[38] with such factors as ionic charge being less important. It is expected that the larger Ce ions ($r_{Ce^{4+}} \simeq 0.08$–0.09Å) will adsorb to Cr_2O_3 grain boundaries in much higher concentrations.

Practical Implications of Superficial Application of Oxides

The beneficial effects of reactive element additions on the oxidation of both Cr_2O_3-forming and Al_2O_3-forming alloys are well known. The use of these elements as alloying additions put certain constraints on melting and forming practices and can be detrimental to alloy mechanical properties. Therefore, methods of obtaining the beneficial effects of the reactive elements by surface treatment are quite attractive. The oxidation rate of Cr_2O_3-forming stainless steels in CO_2 has been markedly reduced by ion implantation of Ce prior to oxidation.[39] Ion implantation is an expensive technique and application of the reactive element as an oxide dispersion or other compound, is preferable, if effective. This approach has been known for many years (e.g., Ref. 40) but has not been applied in a scientific manner. Recently, the oxidation resistance of stainless steels in CO_2 has been improved over long periods by the application of CeO_2 in the form of a nitrate which decomposes on heating[41] and by a sol-gel technique.[42]

The results of the present investigation indicate the oxidation rates of Cr_2O_3-forming alloys can be markedly reduced and the resistance to spalling improved by the superficial application of stable oxide powders prior to oxidation. The nature of the oxide is, however, important as evidenced by the difference in behavior of Fe–Cr alloys coated with MgO as compared to CeO_2. The mechanism proposed in the previous section for the effects of CeO_2 implies that a stable oxide whose cation does not fit well in the Cr_2O_3 lattice should provide optimum results. The amount of oxide or the particle size were not varied in this investigation but it would appear that the finest particle size feasible should be used.

The long-term effects of external application of oxide particles has not been adequately evaluated and the tendency for the acceleration in rate for CeO_2-coated Fe–25Cr at times longer than 100 hr calls this into question, particularly for cyclic conditions. However, the simplicity of the technique and the results reported here and previously[41,42] suggest the technique should be useful for many applications.

SUMMARY

Superficial application of CeO_2 powder was found to produce similar effects on the oxidation behavior of Ni–50Cr alloys as do alloying additions

of Ce. These include: (1) decreased scale growth rate, (ii) increased scale adhesion, and (iii) reduced oxide grain size. Application of Co_3O_4 or Cr_2O_3 powders do not significantly affect the growth rate of Cr_2O_3.

Application of CeO_2 powder to Fe–25Cr decreases the Cr_2O_3 grain size, decreases the amount of Fe oxides in the scale, and decreases the Cr_2O_3 growth rate. Application of MgO powder decreases the oxide grain size and the amount of Fe oxides in the scale but does not reduce the Cr_2O_3 growth rate.

The above observations have been explained by (i) externally applied oxides affecting the nucleation and growth of a fine-grained Cr_2O_3 scale and (ii) oxides with large cations reducing the Cr_2O_3 growth rate by adsorption of the cations to Cr_2O_3 grain boundaries. The thinner, fine-grained scales provide better adhesion. The practical implications of external application of stable oxide powders have been discussed.

REFERENCES

1. S. D. Sehgal and D. Swarup, *Trans. Ind. Inst. Met.* **15**, 177 (1962).
2. T. Nakayama and Y. Watanabe, *Trans. Iron Steel Inst. Jpn*, **8**, 259 (1968).
3. E. J. Felten, *J. Electrochem. Soc.* **108**, 490 (1961).
4. J. E. Antill and K. A. Peakall, *J. Iron Steel Inst.* **205**, 1136 (1967).
5. G. C. Wood and J. Bousted, *Corros. Sci.* **8**, 719 (1968).
6. Y. Nakamura, *Metall. Trans.* **5**, 909 (1974).
7. J. M. Francis and W. H. Whitlow, *J. Iron Steel Inst.* **204**, 355 (1966).
8. J. M. Francis and J. A. Jutson, *J. Iron Steel Inst.* **207**, 639 (1966).
9. V. K. Farafonov, M. M. Shteinberg, Z. G. Tret'yakova, and V. V. Voiner, *Metal Sci. Heat Treat.* 294 (1967).
10. P. Hoch, V. Masarik, and V. Chihal, *Rev. Metall.* **67**, 113 (1970).
11. D. Ignatov and R. Shamgunova, *NASA Tech. Transl.* F-49 (1961).
12. W. C. Hagel, *Trans. Am. Soc. Met.* **56**, 583 (1963).
13. G. M. Ecer and G. H. Meier, *Oxid. Met.* 13, 159 (1979).
14. H. Nagai, T. Murai, and H. Mitani, *Trans. Jpn. Inst. Metals*, **20**, 299 (1979).
15. H. Nagai, T. Murai, and H. Mitani, *Trans. Jpn. Inst. Metals*, **20**, 442 (1979).
16. H. Nagai, M. Okabayashi, and H. Mitani, *Trans. Jpn. Inst. Metals*, **21**, (1980).
17. H. Nagai, T. Murai, and H. Mitani, *Trans. Jpn. Inst. Metals*, **21**, 563 (1980).
18. C. S. Giggins and F. S. Pettit, *Metall. Trans.* **2**, 1071 (1971).
19. H. H. Davis, H. C. Graham, and I. A. Kvernes, *Oxid. Met.* **3**, 431 (1971).
20. G. R. Wallwork and A. Z. Hed, *Oxid. Met.* **3**, 229 (1971).
21. J. Stringer, B. A. Wilcox, and R. I. Jaffee, *Oxid. Met.* **5**, 11 (1972).
22. I. G. Wright, B. A. Wilcox, and R. I. Jaffee, *Oxid. Met.* **9**, 275 (1975).
23. I. G. Wright and B. A. Wilcox, *Oxid. Met.* **8**, 283 (1974).
24. J. Stringer and I. G. Wright, *Oxid. Met.* **5**, 59 (1972).
25. D. P. Whittle and J. Stringer, "The Oxidation Behavior of Cobalt Base Alloys Containing Dispersed Oxides Formed by Internal Oxidation," in *Properties of High Temperature Alloys*, Z. A. Foroulis and F. S. Pettit, eds. (The Electrochemical Society, Princeton, 1977) p. 261.
26. D. P Whittle, M. E. El-Dahshan, and J. Stringer, *Corros. Sci.* **17**, 879 (1977).
27. O. T. Goncel, J. Stringer, and D. P. Whittle, *Corros. Sci.* **18**, 701 (1978).
28. O. T. Goncel, D. P. Whittle, and J. Stringer, *Corros. Sci.* **19**, 305 (1979).
29. H. Nagai and M. Okabayashi, *Trans. Jpn Inst. Metals* **22**, 101 (1981).

30. O. T. Goncel, D. P. Whittle, and J. Stringer, *Oxid. Met.* **15**, 287 (1981).
31. G. M. Ecer and G. H. Meier, *Scripta Metall.* 1189 (1973).
32. G. M. Ecer and G. H. Meier, *Oxid. Met.* **13**, 119 (1979).
33. G. M. Ecer and G. H. Meier, "Oxidation of High-Chromium binary Ni–Cr Alloys and Ternary Alloys Containing Ce, Zr and Ti," in Properties of High Temperature Alloys, Z. A. Foroulis and F. S. Pettit, eds. (The Electrochemical Society, Princeton, 1977), pp. 279–310.
34. Y. Shida, G. C. Wood, F. H. Stott, D. P. Whittle, and B. D. Bastow, *Corros. Sci.* **21**, 581 (1981).
35. D. Delaunay, A. M. Huntz, and P. Lacombe, *Corros. Sci.* **20**, 1109 (1980).
36. P. Kofstad and K. P. Lillerud, *J. Electrochem. Soc.* **127**, 2410 (1980).
37. K. T. Chiang and G. H. Meier, unpublished research, University of Pittsburgh (1981).
38. W. C. Johnson, *Metall. Trans.* **8A**, 1413 (1977).
39. M. J. Bennett, G. Dearnaley M. R. Houlton, R. W. M. Hawes, P. D. Goode, and M. A. Wilkins, *Corros. Sci.* **20**, 73 (1980).
40. L. B. Pfeil, U.K. Patent no. 574088 (1945).
41. C. Tyzack, H. E. Cowen, M. Farrow, P. B. Longton, and W. H. Whitlow "Effect of Surface Treatment with Rare Earth Oxide on the Oxidation of 20/25/Nb Stainless Steel," Paper 29 BNES International Conference on Corrosion of Steels in Co_2, Reading, (September 1974).
42. M. J. Bennett, M. R. Houlton, and J. B. Price, "New Ceramic Coatings for High Temperature Gas-Cooled Reactor Materials Protection," paper presented in IAEA Specialists Meeting on High Temperature Metallic Materials for Application in Gas-Cooled Reactions, May, 1981.